

# Resonance Related Spiral Substructure in a Galactic Gaseous Disk

Miguel A. Yáñez, Michael L. Norman

*Center for Astrophysics and Space Sciences, University of California at San Diego, La Jolla, CA 92093*

myanez@ucsd.edu

mlnorman@ucsd.edu

Marco A. Martos

*Instituto de Astronomía, Universidad Nacional Autónoma de México A. P. 70-264, México 04510, D. F., México*

marco@astroscu.unam.mx

and

John C. Hayes

*Lawrence Livermore National Laboratory, Livermore, CA 94550*

jchayes@llnl.gov

## ABSTRACT

We use high resolution ( $2048^2$  zones) 2D hydrodynamic simulations to study the formation of spiral substructure in the gaseous disk of a galaxy. The obtained gaseous response is driven by a self-consistent non-axisymmetric potential obtained from an imposed spiral mass distribution. We highlight the importance of ultraharmonic resonances in generating these features. The temporal evolution of the system is followed with the parallel ZEUS-MP code, and we follow the steepening of perturbations induced by the spiral potential until large-scale shocks emerge. These shocks exhibit bifurcations that protrude from the gaseous arms and continue to steepen until new shocks are formed. When the contribution from the spiral potential relative to the axisymmetric background is increased from our default value, spurs protrude from the main arms after several revolutions of the gaseous disk. Such spurs overlap on top of the aforementioned shocks. These results support the hypothesis that a complicated gaseous response can coexist with an orderly spiral potential term, in the sense that the underlying background potential can be smooth yet drive a gaseous response that is far more spatially complex.

*Subject headings:* large scale galactic shocks: general — ultraharmonic resonances, interarm features, branches: individual(branches and spurs)

## 1. Introduction

Young stars, H II regions and OB associations delineate the structure that gives its name to spiral galaxies (Elmegreen 1981; Vallée 2002, 2005). This implies a correlation between the spiral structure and the process of star formation. The density wave theory attempts to explain the large-scale structure of these galaxies in terms of a wave propagating in the disk of stars. Yet this stellar wave alone cannot directly explain the narrow spiral arms as delineated by the products of star formation.

Fujimoto (1968) first proposed that the dust lanes observed on the concave side (inside corotation) of spiral arms might be the result of a Galactic shock. Large scale shocks propagating in the gaseous layer of the Galaxy could induce a sudden compression of the interstellar medium (ISM) and trigger the star formation process. Since the temporal scales involved in this process are large (of the order of the Galactic rotation period), an isothermal approximation of the ISM is a first step in modeling the gaseous response, thus rendering a highly compressible-supersonic medium in which a small amplitude disturbance, such as that provided by an underlying spiral potential, may steepen into a shock wave.

In a semi-analytical study of the gas flow in spiral density waves, Roberts (1969) found nonlinear steady-state solutions containing shocks. On the basis that these shocks were coincident with the imposed perturbing potential minima, he argued that the density jump could trigger star formation, and in this way narrow bands of young stars could delineate the spiral arms.

Shu et al. (1973) studied the gas flow in the context of the spiral density wave by adopting a two phase model for the ISM. In their study they carried out a slightly nonlinear analysis of such flow and found that, at certain points in their solution, the amplitude became infinite, and they called these positions ultraharmonic resonances. They argued that additional prominent features could appear as a consequence of the ultraharmonic resonances, for instance: they found a secondary compression associated with the first one.

However, these studies were carried out assuming steady state flow and tightly wound spirals. By removing the first constraint, Woodward (1975) showed how the convective steepening of the initial perturbation leads to large-scale shock formation (as a response to the driving potential) in a gaseous layer initially in circular orbit. He also found the effect of the first ultraharmonic resonance as a secondary peak in the density field, but numerical

viscosity in his calculations inhibited the formation of secondary shocks.

In two papers, Contopoulos & Grosbøl (1986, 1988) removed the second constraint and showed that nonlinear effects are not negligible in open spirals. Using numerical calculations, they demonstrated that for open spirals the effect of the first ultraharmonic resonance (which they call the 4:1 resonance) is such that stellar orbits do not support the spiral perturbation beyond the position of this resonance and hence the length of the stellar spiral arms is limited by this position. In an analytical study of the effects of the ultraharmonic resonances, Artymowicz & Lubow (1992) explained this result as a cumulative effect of higher-order resonances between 4:1 and the corotation radius. They further argued that in the vicinity of the former the gas response is such that it looks like a 4-arm structure with a smaller pitch angle than that of the original two-arm pattern.

It is clear that, due to the nature of the problem, the highly nonlinear phenomena associated with the gaseous response to a spiral density wave are best studied via numerical simulations. Results so obtained add interarm features and spiral substructure on top of large scale shocks. Patsis et al. (1997) found that in open spirals a bifurcation of the main spiral arms takes place at the 4:1 resonance position. By analyzing numerical experiments that include self-gravity in the study of the effects of the ultraharmonic resonances on gaseous disks, Chakrabarti et al. (2003, from here on CLS03) found secondary compressions, associated with the first ultraharmonic resonance, in models with a low Toomre parameter,  $Q$ , which were evolved only for a few revolutions of the disk. These compressions eventually became branches. In high- $Q$  models, evolved for several revolutions they found the appearance of leading structures which they identified with spurs. However, spurs and branches not related to resonances have also been obtained in numerical simulations. By taking into account frozen magnetic fields and self-gravity in their local arm simulations, Kim & Ostriker (2002, 2006) showed that gaseous spurs form as a consequence of gravitational instability inside the spiral arms, a result confirmed with global 2D simulations by Shetty & Ostriker (2006). In those simulations spurs jut out of the spiral arms at regular intervals.

In this paper we carry out two dimensional, global, high resolution hydrodynamic simulations to further study the formation of spiral substructure in galactic gaseous disks. Our approach differs from previous work in that we employ a self-consistent model for the spiral stellar potential (in the orbital sense). This potential accounts for its own self-gravity and thus is no longer a local arm approximation to the driving term, making it more appropriate for simulations of open galaxies. This paper is organized as follows: in §2 we describe the potential we employ, in §3 we present the obtained gaseous response and the type of substructure related to it, in §4 we discuss the results and compare with previous work, and in §5 we present our conclusions.

## 2. Modeling

### 2.1. The potential

We employ a potential that consists of two parts. The first one is the axisymmetric background contribution, taken from Allen & Santillán (1991). This model assembles contributions from a bulge and a flattened disk in the way proposed by Miyamoto and Nagai (1975), plus a massive spherical dark halo. This potential was chosen for its simplicity and easy mathematical manipulation. It renders a flat rotation curve of about  $200 \text{ km s}^{-1}$  at a moderate radius and provides reasonable values for Galactic parameters.

The nonaxisymmetric contribution is more delicate. The usual approach to model this term is via a logarithmic spiral potential. The rationale underlying this choice is two-fold: first, from the mathematical point of view it is tractable, and second, no simpler form is known to represent this term. Yet, this choice has some limitations. It assumes that only local effects of the potential can influence the gas dynamics; that is, it considers the potential minima to be in the geometrical center of the spiral arms. Such a potential is self-consistent only for small pitch angles and does not consider its own self-gravity. To remove such constraints and perform more adequate simulations in the presence of an open spiral, we choose a self-consistent potential (in the orbital sense) and with it performed our numerical experiments. We employ a model derived from an imposed stellar spiral mass distribution given by Pichardo et al. (2003). In this paper self-consistency refers to the reinforcement of the spiral potential by the stellar orbits, i.e., the orbits of the stars respond to the spiral potential in such a way as to reform the spiral locus of the initially imposed potential.

In order to obtain the potential given by an imposed open spiral mass distribution, Pichardo et al. (2003) selected a possible spiral locus for the morphology of the Galaxy. Then they place a series of oblate spheroids along this locus to fit the mass distribution of our Galaxy. In this way the total potential at a given point is found by adding the contributions of every spheroid at that same point. The characteristics of the spheroids are as follows: the minor axis of the spheroids is perpendicular to the Galactic plane and extends up to 0.5 kpc. The major semiaxes have a length of 1 kpc and lie in the Galactic plane. The locus on which they are placed fits the K band data of Drimmel (2000) with a pitch angle of  $15.5^\circ$ . The central density of the spheroids follows an exponential law with a scale length of 2.5 kpc, approximately that of the near-infrared Galactic disk (Freudenreich 1998). The self-consistency study of the potential was carried out following the same procedure as Contopoulos and Grosbøl (1986). To obtain the density response to the spiral perturbation, Pichardo et al. (2003) assume that stars with circular orbits and rotating in the same sense as the spiral pattern are trapped around the corresponding central periodic orbit in the

presence of the spiral perturbing term. They compute a series of central periodic orbits and find the density response along their extension. They match the density response maxima with the center of the assumed spiral arms (the imposed spiral locus) and whenever they match, self-consistency can be claimed. In this way they showed that self-consistency of their models was a function of two parameters: the angular pattern speed ( $\Omega_p$ ) and the ratio of mass contained in the arms to that contained in the disk,  $M_A/M_D$ . The best-fit values of these parameters to achieve self-consistency were  $\Omega_p = 20 \text{ km s}^{-1} \text{ kpc}^{-1}$  and  $M_A/M_D = 0.0175$ , respectively.

## 2.2. Model Parameters

Our numerical calculations compute the 2D hydrodynamic gaseous response to an external, fixed, spiral mass distribution in a 3D galactic disk model. We performed our simulations in a frame that corotates with the imposed spiral pattern. The gaseous layer was initialized in centrifugal equilibrium with the axisymmetric potential and then the spiral term was turned on. The nonaxisymmetric term was modeled as a rigidly rotating potential with an angular speed  $\Omega_p$ . We investigated spiral substructure formation by solving the hydrodynamical equations in polar coordinates in a frame rotating with this prescribed pattern speed. In this frame the hydrodynamical equations are

$$\frac{\partial \rho}{\partial t} + \nabla \cdot (\rho \mathbf{v}') = 0 \quad (1)$$

$$\rho \left[ \frac{\partial \mathbf{v}'}{\partial t} + (\mathbf{v}' \cdot \nabla) \mathbf{v}' \right] = -\nabla p - \rho (\nabla \Phi_{as} + \nabla \Phi_s + 2\Omega_p \times \mathbf{v}' + \Omega_p \times (\Omega_p \times r)) \quad (2)$$

$$\rho \left[ \frac{\partial}{\partial t} \left( \frac{e}{\rho} \right) + \mathbf{v}' \cdot \nabla \left( \frac{e}{\rho} \right) \right] + p \nabla \cdot \mathbf{v}' = 0 \quad (3)$$

In these equations  $\rho$  is the gas density,  $\mathbf{v}'$  the velocity in the rotating frame,  $p$  the pressure,  $\Phi_{as}$  is the background axisymmetric potential,  $\Phi_s$  the potential associated with the imposed spiral mass distribution, and  $e$  the gaseous internal energy.

An idealized ISM was assumed for these simulations in that we adopt an effectively isothermal equation of state ( $\gamma = 1.01$ ) for the system. A constant sound speed,  $c_s$ , of  $7 \text{ km s}^{-1}$  was used. We followed the evolution of the gaseous response for several rotations; one

rotation is completed after  $t_{orb} = 2\pi/\Omega_0$  at a fiducial radius  $R_0$ . We present simulations that evolve for 10 revolutions.

The effect of the first ultraharmonic resonance was studied by changing  $\Omega_p$  so that the location of the resonance lay either inside or outside the maximum radius of the spiral mass distribution (12 kpc). This was accomplished by selecting  $\Omega_p$  values of 20 and 10 km s<sup>-1</sup> kpc<sup>-1</sup>, respectively. We also explored the effects of a stronger spiral potential relative to the background axisymmetric contribution. Since the driving term we use is obtained from an imposed mass distribution, we may control the relative force perturbation from the spiral potential by adjusting the mass contained in the spiral arms. Using a constant pitch angle of 15.5° for the spiral locus, force perturbations of 3% and 10% are obtained from mass ratios for the spiral arms to the disk ( $M_A/M_D$ ) of 0.0175, 0.05, respectively.

We follow the temporal evolution of the gaseous disk by solving the hydrodynamical equations (1)-(3) in cylindrical polar coordinates (Z-R- $\phi$ ) with the ZEUS-MP code (Hayes et al. 2006). ZEUS-MP differs from previous implementations of the ZEUS code in that it is designed for numerical calculations on massively parallel computing platforms. ZEUS-MP solves the equations of radiation magnetohydrodynamics in 1D, 2D or 3D in cartesian, cylindrical or spherical coordinates. The code has been tested against an extensive bank of test problems documented in Hayes et al. (2006). For our simulations, we neglect magnetic fields and radiation transport.

Our model uses a computational mesh covering  $2\pi$  radians in azimuth and extending from 1 to 15 kpc in radius. Several boundary conditions were tried to ensure that wave reflections at the boundaries are not affecting our results. Inner inflow conditions prevent wave reflections from infalling gas and outer open conditions prevent gas from becoming stagnant. 2D models were computed in cylindrical polar coordinates by modifying the code so that symmetry was imposed along the leading (Z) coordinate and all acceleration terms along the Z axis in the momentum equation were zeroed. We present numerical experiments in a computational mesh with  $2048^2$  zones in R and  $\phi$ ; we are thus able to resolve the formation of substructure on scales  $\leq 10$  pc in the radial direction. The minimum and maximum resolution achieved on the computational grid are 21 pc<sup>2</sup> and 293 pc<sup>2</sup> respectively.

### 3. RESULTS

In Figure 1 we show snapshots of the density distribution corresponding to the case  $\Omega_p = 20$  km s<sup>-1</sup> kpc<sup>-1</sup>. We observe that at  $t/t_{orb} = 0.1$  the gas responds to the external potential by tracing the potential minima, clustering around them. At this time the gas is

adjusting to the potential and the density perturbation is steadily steepening in response to the spiral arms. Slightly later, at  $t/t_{orb} = 0.26$ , the recently formed gaseous arms begin to bifurcate. This bifurcation occurs in the vicinity of the first ultraharmonic resonance at a radius of 7 kpc, which is marked with a dashed line. Gas continues to accumulate around the potential minima and the newly formed bifurcations until two pairs of large-scale shock waves are formed. We show the final steady-state configuration in the third snapshot of Figure 1. Two shock waves trace the underlying spiral potential while the other two shock waves are the result of the steepening of the bifurcations. Similar results were presented by Martos et al. (2004) at lower resolution and with a previous version of the code. In Figure 2 we have plotted a density cut at a radius of 6 kpc, in order to illustrate the arm to interarm contrast at evolution times corresponding to snapshots (b) and (c) of Figure 1. The arm to interarm contrast is a function of radius and time, but generally speaking we can state that the shocks associated with the imposed spiral mass distribution have a higher contrast and are more extended in the radial direction than the shocks associated with the bifurcations. The compressions,  $\rho/\rho_0$ , induced by these shocks have a peak around 8, in the inner regions, and 3 on average. The new shocks arising from bifurcations of the first shocks induce lower compressions with average values around 2. These shocks also have a lower pitch angle and their radial extent is limited by the first ultraharmonic resonance position. They can be found in the range of 6-7.5 kpc.

### 3.1. Varying $\Omega_p$

In order to emphasize the importance of the first ultraharmonic resonance on the bifurcation of the spiral arms, we have performed simulations where the position of this resonance has been shifted beyond the termination of the imposed spiral mass distribution. If we maintain fixed all other parameters and vary  $\Omega_p$  from 20 to 10  $\text{km s}^{-1} \text{ kpc}^{-1}$  then the new position of the first ultraharmonic resonance is 14 kpc. In Figure 3 we show the density distributions for this case.

The evolution of the system is similar to before: the induced perturbations in the gas steepen into large-scale shock waves and accumulate around the potential minima. In snapshot (b) we observe transient substructure emerging as waves propagate radially. After a few revolutions of the potential, this substructure is smoothed. In snapshot (c) only a two-arm gaseous response remains and the density peaks have been shifted downstream relative to the previous case. We also observe waves propagating from the tips of the arms radially outwards. These waves have been reflected in the corotation region and amplified, yet they do not add to the large-scale shocks and remain in an intermediate region between the end

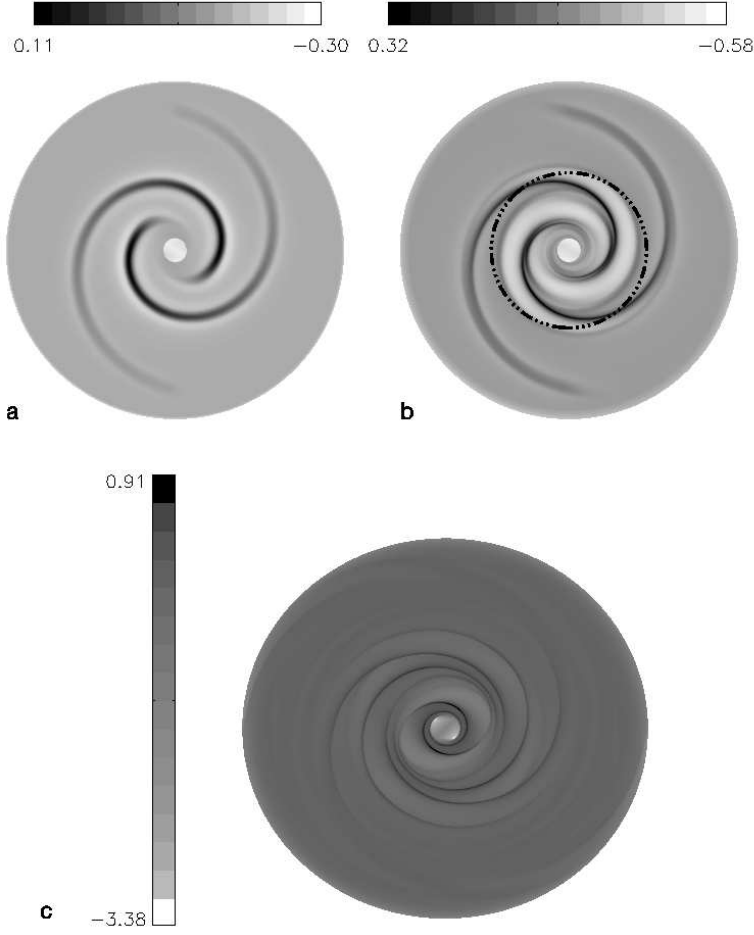


Fig. 1.— Density snapshots for the case  $\Omega_p=20 \text{ km s}^{-1} \text{ kpc}^{-1}$ . Surface density at (a)  $t/t_{orb}=0.1$ , (b)  $t/t_{orb}=0.26$  the position of the first ultraharmonic resonance is marked by a dashed line, and (c)  $t/t_{orb}=8.25$ . The density scale is shown in units of  $\log \Sigma/\Sigma_0$ . The outer boundary for this simulation is located at 15 kpc.



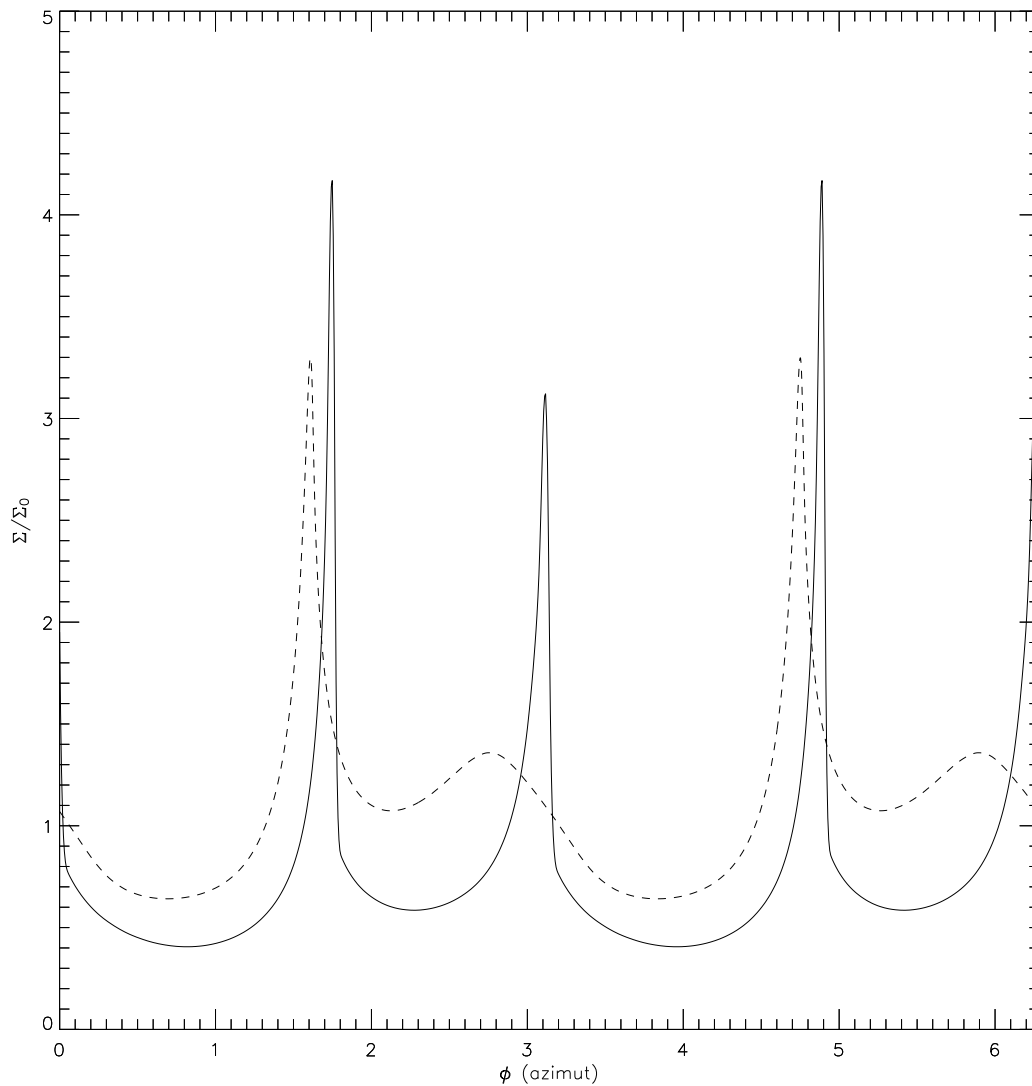


Fig. 2.— Density cut at 6 kpc. We have plotted the ratio of density to initial density, to show the arm to interarm contrast attained in this simulation. The dotted line represents density contrasts at  $t/t_{orb} = 0.26$  and the continuous line at  $t/t_{orb} = 8.5$ .

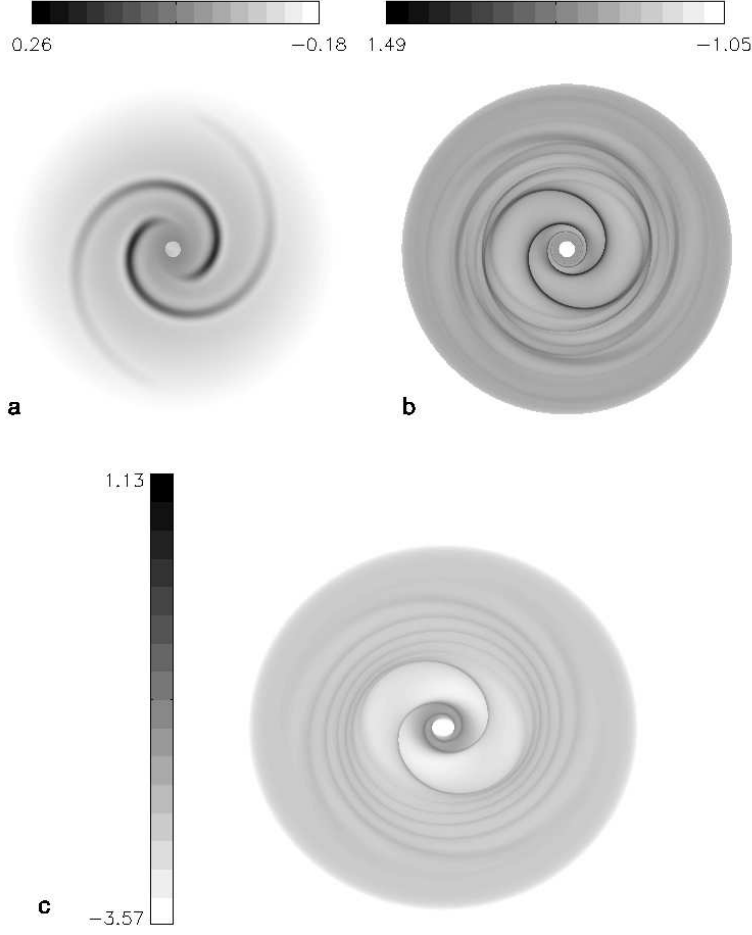


Fig. 3.— Density distribution snapshots for the case  $\Omega_p = 10 \text{ km s}^{-1} \text{ kpc}^{-1}$ . Inner boundary is at 1 kpc and outer radius at 22 kpc. The position of the first ultraharmonic resonance is 14 kpc. Surface density at (a)  $t/t_{orb} = 0.05$ , (b)  $t/t_{orb} = 1.03$ , and (c)  $t/t_{orb} = 10$ . The density scale is shown in units of  $\log \Sigma / \Sigma_0$ .

of the imposed potential and the corotation radius.

### 3.2. Higher Forcing

A higher forcing case corresponds to either a more massive or a more open spiral driving term. Since the potential model employed is derived from an imposed spiral mass distribution, we increased the mass in the spiral distribution to achieve a higher forcing term. In the case described here we adopted a mass ratio of the arms to the disk of  $M_A/M_D=0.05$ . With this parameter we have an average relative force perturbation of  $\sim 10\%$ . The gaseous response presented in Figure 4 is such that, initially, density enhancements around the potential minima are obtained. At  $t/t_{orb} = 0.26$  (snapshot a) branches begin to emerge near the first ultraharmonic position (at 7 kpc) and eventually interact with the already formed gaseous arms. Waves reflect from the inner Lindblad resonance (at 3 kpc) and the corotation radius (located at 11 kpc) and interact with the existing density enhancements as they steepen. In this way, we obtain a temporary ragged appearance, illustrated in snapshot (b) at  $t/t_{orb}=1$ . The system, however, evolves to a quasi-steady state, and this rich substructure is eventually sheared away. In this simulation the shock structure does not remain fixed; the shocks oscillate and so does the spiral substructure. We followed this simulation to  $t/t_{orb}=10$ , and both oscillations and overall shock structure were preserved. In this sense we say that system achieved a quasi-steady state.

An interesting outcome of this simulation is the appearance after a few revolutions of substructure in the internal regions of the computational mesh. Short streams extend out from the main gaseous arms; these streams are small compared with the bifurcations and have a greater pitch angle. Because these characteristics match those given by Elmegreen (1981) to classify spurs, so we will refer to them as such. In snapshot (c) we present the final configuration of the system which displays the previously noted 4-arm shock structure plus spurs at an evolution time of  $t/t_{orb}=10$ . The spurs are marked with draw-in arrows. These spurs protrude from the main arms into the already steepened branches, and as can be seen in this snapshot, they wind in an opposite sense to the general gas rotation. The spurs are symmetric with respect to the main arms and originate close to inner Lindblad resonance.

## 4. Discussion

Analytical work on the gaseous disk response to an external driving spiral potential by Shu et al. (1973) and Artymowicz & Lubow (1992) highlighted the importance of the

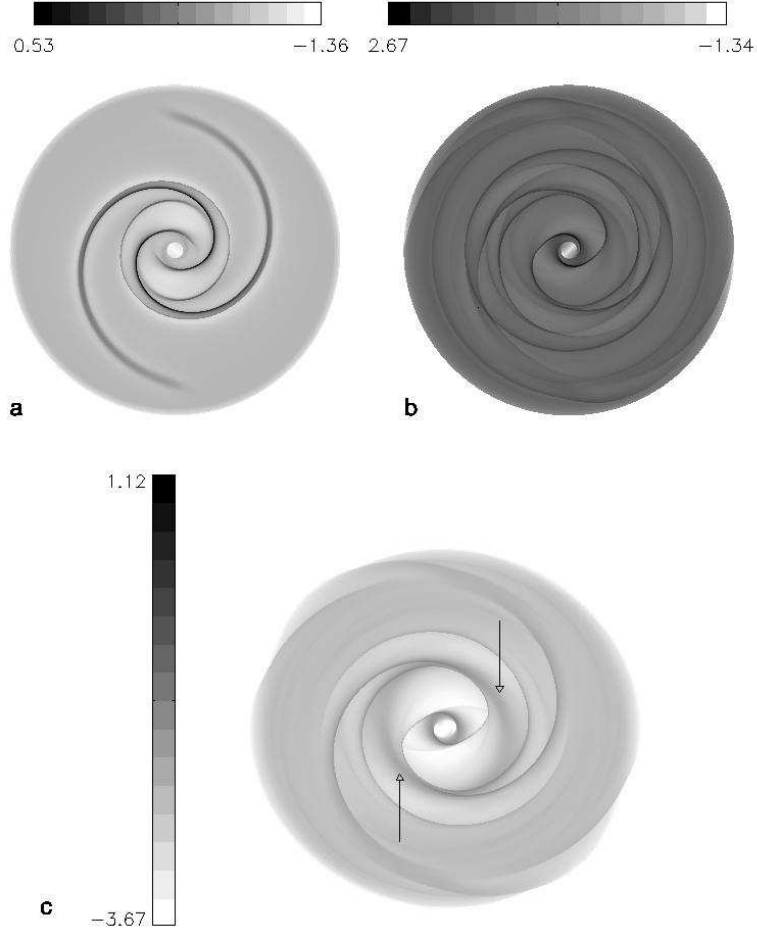


Fig. 4.— Density contours snapshots for the case  $M_A/M_D=0.05$ . Surface density at (a)  $t/t_{orb}=0.26$ , (b)  $t/t_{orb}=1.55$ , and (c)  $t/t_{orb}=10$ . Spurs are delimited with solid lines, protruding from spiral arms. The density scale is shown in units of  $\log \Sigma/\Sigma_0$ .

first ultraharmonic resonance as the main generator of spiral substructure. Those studies concluded that in a slightly nonlinear regime a second compression emerged in a gaseous disk that could account for observed spiral substructure. But a more complete study is necessary to identify the effect of resonances in a fully nonlinear regime. Due to the nature of the equations governing the evolution of such a disk, this task is best accomplished using numerical simulations.

Numerical work on this subject by Patsis et al. (1997) and CLS03 revealed that substructure arising in gaseous disks is related to ultraharmonic resonances. Branches and spurs have been obtained in self-gravitating models which are stable against axisymmetric perturbations (i.e. with a Toomre parameter greater than 1). These spurs and branches have also been obtained in magnetized disks in the absence of self-gravity, but unrelated to ultraharmonic resonances and caused by a magneto-Jeans instability (Kim & Ostriker 2002, 2006).

The gaseous response we have presented resembles that of previous numerical work: the initial response tends to associate with the underlying potential, and once gaseous arms have formed, branches begin to protrude from them. But in our simulations these branches continue to steepen, leading to the formation of new shock waves, with lower radial extension, pitch angle and Mach number, but large-scale shock waves nevertheless. The role of the first ultraharmonic resonance is such that, if absent from the region of influence of the spiral term, no such additional shocks are formed.

We also performed simulations with high forcing and obtained additional substructure: gaseous spurs. These spurs protrude from the arms after several revolutions and are not a transient feature. We wish to note that these results were obtained without self-gravity in the gaseous disk and that spurs and bifurcations are obtained in the same long-timescale simulation. Such spurs wind in the opposite sense to the arms rotation and are restricted to an area close to the inner Lindblad resonance. CLS03 also obtained gaseous spurs employing a nonlinear perturbing potential with high forcing, but in their simulations they had to use a disk very stable against axisymmetric perturbations and thus they could not obtain branches and spurs in the same simulation. In our case we use a spiral term that ensures self-consistency and employ the maximum value for forcing (5%, a similar value as that used by CLS03 to obtain spurs) that still renders a self-consistent driving term according to Pichardo et al (2003). Our driving term and our algorithms to calculate the gaseous response have proven robust enough as to allow the development of branches and spurs in the same run. The high numerical resolution and consequent low numerical dissipation of our simulation may also have been important in obtaining this result. CLS03 include self-gravity in the gaseous layer and the spurs they obtain are more pronounced. Although we demonstrated

that these features can emerge in the absence of self-gravity in the gaseous layer, we are well aware that self-gravity in the gas will enhance the features we have found giving rise to higher arm-interarm density contrasts.

It is worth remarking that the simulations presented here can be evolved for several revolutions of the driving term (more than  $t/t_{orb} = 10$ ) and eventually achieve a steady state. Yet the isothermal condition we assumed can only reproduce the formation of substructure, but not its subsequent fragmentation. To reproduce the latter we need to adopt a more realistic treatment of the ISM, with special attention to its thermodynamic properties. Another line of improvement is suggested by previous work showing that the inclusion of frozen magnetic fields leads to the formation of additional substructure. We defer a discussion of the role of magnetic fields to a future paper.

## 5. Conclusions

A fully nonlinear treatment of the propagation of spiral density waves in a gaseous disk is tractable using numerical simulations. By considering an open spiral, in the absence of self-gravity in the gaseous layer, we are able to obtain rich substructure associated with an external spiral potential. Our work differs from other published results in that we employ a self-consistent driving term that considers its own gravity and removes the local arm approximation. We have presented experiments showing the formation of a four-arm structure in response to a two-arm driving pattern. Initially the gas accumulates in the potential minima. After some time the gas responds to resonances and the main arms bifurcate. These features have a considerable azimuthal extension and continue to steepen with time. Eventually a four-arm shock structure emerges, in the gaseous layer that coexist with the underlying two-arm potential, made up by the stars. This result appears to agree with observational data published by Drimmel (2000) where he concludes that, using optical tracers, the spiral structure in our Galaxy is best fitted by a four-arm structure, while in the infrared a two-arm structure dominates.

If we place the first ultraharmonic resonance outside the region of influence of the spiral (in our case by changing the value of  $\Omega_p$ ) the main arms do not bifurcate and large-scale shocks are the only induced response in the gaseous layer. In this way we show that if the first ultraharmonic resonance is placed outside the region of influence of the perturbing term, no spiral substructure appears, thus emphasizing the connection between this resonance and the bifurcations of the gaseous arms.

If we combine the effects of the resonances with a large forcing amplitude we obtain, on

top of this four-arm structure, spurs protruding from the main arms in a region between the inner Lindblad resonance and the first ultraharmonic resonance. Overlapping of nonlinear effects take place in our long-timescale global simulations, showing that an orderly spiral density wave potential can produce a gaseous response that is strongly disordered.

The inclusion of additional processes such as magnetic fields, self-gravity for the gaseous layer, and thermal processes in the ISM may lead to the appearance of additional substructure and their consequent fragmentation into bound condensations. Numerical experiments addressing these topics are needed in order to improve our understanding of the global ISM in galaxies and its relation to large-scale processes.

M. Yáñez and M. Martos want to thank the UCMEXUS-CONACYT fellowship program for economic support. M. Martos thanks the CASS-UCSD for their hospitality during a sabbatical visit which helped pursue this project. The numerical simulations were carried out on the DataStar system at the San Diego Supercomputer Center with LRAC allocation MCA98N020.

## REFERENCES

- Allen, C. and Santillán, A. 1991, *Rev. Mexicana Astron. Astrofis.*, 22, 255
- Artymowicz, P. and Lubow, S. H. 1992, *ApJ*, 389, 129
- Chakrabarti, S., Laughlin, G. and Shu, F. H. 2003, *ApJ*, 596, 220
- Contopoulos, G. and Grosbøl, P. 1986, *A&A*, 155, 11
- Contopoulos, G. and Grosbøl, P. 1988, *A&A*, 197, 83
- Drimmel, R. 2000, *A&A*, 117, 89
- Elmegreen, D. M. 1981, *ApJS*, 47, 229
- Freudenreich, H. T. 1998, *ApJ*, 492, 495
- Fujimoto, M. 1968, in *IAU Symposium* No. 29, p. 453
- Hayes, J. C., Norman, M. L., Fiedler, R. A., Bordner, J. O., Li, P. S., Clark, S. E., ud-Doula, A. and Mac Low, M. 2006, *ApJS*, 165, 188
- Kim, W. T. and Ostriker, E. 2002, *ApJ*, 570, 132

- Kim, W. T. and Ostriker, E. 2006, *ApJ*, 646, 213
- Martos, M., Hernandez, X., Yáñez, M., Moreno, E. and Pichardo, B. 2004, *MNRAS*, 350, L47
- Miyamoto, M. and Nagai, R. 1975, *PASJ*, 27, 533
- Patsis, P. A., Grosbøl, P. and Hiotelis, N. 1997, *A&A*, 323, 762
- Pichardo, B., Martos, M., Moreno, E. and Espresate, J. 2003, *ApJ*, 582, 230
- Roberts, W. W. 1969, *ApJ*, 158, 123
- Shetty, R. and Ostriker, E. 2006, *ApJ*, 647, 997
- Shu, F. H., Milione, V. and Roberts, W. W. 1973, *ApJ*, 183, 819
- Vallée, J. P. 2002, *ApJ*, 566, 261
- Vallée, J. P. 2005, *ApJ*, 130, 569
- Woodward, P. 1975, *ApJ*, 195, 61